

FIG. 1. Collisionally unstable evolution in an isotropic calculation:  $n_{\nu_e}$  (thick black curve),  $n_{\bar{\nu}_e}$  (medium),  $n_{\nu_x} = n_{\bar{\nu}_x}$  (thin), and neutrino coherence density  $|\mathbf{P}_T|/2$  (teal). For comparison, virtually no flavor conversion or coherence development takes place under collisionless conditions or when  $\Gamma$  and  $\bar{\Gamma}$  are artificially equated. In the case shown, *decoherent* interactions drive the *growth* of flavor coherence.

relax the system differently. Ignoring feedback from flavor conversion,  $\Gamma_{AE}$  returns the system to the classical equilibrium set by the composition of the environment;

$\Gamma_{CC}$  pushes the system toward kinetic equilibrium; and  $\Gamma_{NC}$ , because it leaves flavor coherence intact during interactions, redistributes flavor states over momentum. In an isotropic and monochromatic setting,  $\Gamma_{NC}$  has no effect.

Decomposing the density matrix using  $\rho = (P_0 + \mathbf{P} \cdot \boldsymbol{\sigma})/2$ , with neutrino-number scalar  $P_0$  and polarization vector  $\mathbf{P}$ , the equations of motion become

$$\begin{aligned} \dot{\mathbf{P}} &= \omega \mathbf{B} \times \mathbf{P} + \mu (\mathbf{P} - \bar{\mathbf{P}}) \times \mathbf{P} - \Gamma_+^{CC} \mathbf{P}_T \\ &\quad + \Gamma_+^{AE} (\mathbf{P}^{AE} - \mathbf{P}) + \Gamma_-^{AE} (P_0^{AE} - P_0) \mathbf{z} \\ \dot{P}_0 &= \Gamma_+^{AE} (P_0^{AE} - P_0) + \Gamma_-^{AE} (P_z^{AE} - P_z), \end{aligned} \quad (3)$$

where  $\Gamma_{\pm}^P = (\Gamma_e^P \pm \Gamma_x^P)/2$ . The antineutrino equation is obtained by sending the vacuum Hamiltonian vector  $\omega \mathbf{B} \rightarrow -\omega \mathbf{B}$  and putting bars over all rates and vectors except those in the factor  $\mathbf{P} - \bar{\mathbf{P}}$ . The matter potential  $\lambda = \sqrt{2}G_F n_e$  has been dropped because it does not affect stability [17]. With the chosen convention,  $\mu = \sqrt{2}G_F$ .

Although absorption and emission rates are flavor-dependent, the emergence of instabilities is more transparent (and not fundamentally changed) if we take  $\Gamma_e^{AE} = \Gamma_x^{AE}$ . The total number densities of neutrinos and antineutrinos are then conserved. Letting  $\Gamma^P = \Gamma_+^P$  and switching to the sum and difference vectors  $\mathbf{S} = \mathbf{P} + \bar{\mathbf{P}}$  and  $\mathbf{D} = \mathbf{P} - \bar{\mathbf{P}}$ , we have

$$\begin{aligned} \dot{\mathbf{S}} &= \omega \mathbf{B} \times \mathbf{D} + \mu \mathbf{D} \times \mathbf{S} + \frac{\Gamma^{AE} + \bar{\Gamma}^{AE}}{2} (\mathbf{S}^{AE} - \mathbf{S}) + \frac{\Gamma^{AE} - \bar{\Gamma}^{AE}}{2} (\mathbf{D}^{AE} - \mathbf{D}) - \frac{\Gamma^{CC} + \bar{\Gamma}^{CC}}{2} \mathbf{S}_T - \frac{\Gamma^{CC} - \bar{\Gamma}^{CC}}{2} \mathbf{D}_T \\ \dot{\mathbf{D}} &= \omega \mathbf{B} \times \mathbf{S} + \frac{\Gamma^{AE} - \bar{\Gamma}^{AE}}{2} (\mathbf{S}^{AE} - \mathbf{S}) + \frac{\Gamma^{AE} + \bar{\Gamma}^{AE}}{2} (\mathbf{D}^{AE} - \mathbf{D}) - \frac{\Gamma^{CC} - \bar{\Gamma}^{CC}}{2} \mathbf{S}_T - \frac{\Gamma^{CC} + \bar{\Gamma}^{CC}}{2} \mathbf{D}_T. \end{aligned} \quad (4)$$

Subscript  $T$  indicates that only the part of the vector transverse to the flavor axis is being considered. At this point it begins to become clear how collisions might do more than simply decohere flavor states: the  $\Gamma - \bar{\Gamma}$  terms couple  $\mathbf{S}$  and  $\mathbf{D}$  to one another.

From here on we let  $\Gamma = \Gamma^{AE} + \Gamma^{CC}$ . Now suppose that  $\mu \gg \omega, \Gamma, \bar{\Gamma}$ . For a system that does not support the bipolar instability, the salient effect of the oscillation terms is to cause  $\mathbf{S}$  and  $\mathbf{D}$  to undergo synchronized motion around  $\mathbf{B}$  [17, 18]. In a dense matter background, the vectors remain close to the flavor axis and, to a first approximation, the oscillation terms can simply be dropped. Assuming that  $|(\Gamma - \bar{\Gamma})\mathbf{S}| \gtrsim |(\Gamma + \bar{\Gamma})\mathbf{D}|$ , we obtain

$$\ddot{\mathbf{S}}_T + \frac{\Gamma + \bar{\Gamma}}{2} \dot{\mathbf{S}}_T - \left( \frac{\Gamma - \bar{\Gamma}}{2} \right)^2 \mathbf{S}_T \cong 0. \quad (5)$$

Solutions are exponential, and  $\Gamma \neq \bar{\Gamma}$  is required for one of them to be growing.

An instability criterion follows from the assumption

that  $|(\Gamma - \bar{\Gamma})\mathbf{S}| \gtrsim |(\Gamma + \bar{\Gamma})\mathbf{D}|$ . In a situation with  $\Gamma > \bar{\Gamma}$  and a number-density hierarchy  $n_{\nu_e} > n_{\bar{\nu}_e} > n_{\nu_x} \approx n_{\bar{\nu}_x}$ , instability is predicted for

$$\mathcal{R} \equiv \frac{n_{\bar{\nu}_e} - n_{\bar{\nu}_x}}{n_{\nu_e} - n_{\nu_x}} \gtrsim \frac{\bar{\Gamma}}{\Gamma} \equiv \mathcal{R}_{\text{crit}}. \quad (6)$$

Numerical tests support the accuracy of this criterion. As  $\mathcal{R}$  decreases toward  $\mathcal{R}_{\text{crit}}$ , the time elapsed before instability sets in grows longer. Below  $\mathcal{R}_{\text{crit}}$  the instability has apparently vanished.

The system admits of another collisional instability. Synchronization of  $\mathbf{S}$  and  $\mathbf{D}$  implies that

$$\dot{\mathbf{D}}_T \cong \left( \pm \frac{\Gamma - \bar{\Gamma}}{2} \frac{|\mathbf{S}|}{|\mathbf{D}|} - \frac{\Gamma + \bar{\Gamma}}{2} \right) \mathbf{D}_T, \quad (7)$$

with the upper (lower) sign corresponding to  $\mathcal{R} > 1$  ( $\mathcal{R} < 1$ ). If  $\mathcal{R} < 1$  and  $\bar{\Gamma} > \Gamma$ , or if  $\mathcal{R} > 1$  and  $\bar{\Gamma} < \Gamma$ , then an exponentially growing solution is possible, but it is less likely to be of relevance to supernovae.

*An illustrative calculation.*—Figure 1 presents the numerical solution of Eqs. (3) using parameters motivated by realistic conditions inside a core-collapse supernova. To be definite, the chosen values emulate those found at, say, a post-bounce time of  $\sim 200$  ms and a radius of  $\sim 40$  km: namely, a density of  $10^{12}$  g/cm<sup>3</sup>, a temperature  $T = 7$  MeV, an electron chemical potential  $\mu_e = 20$  MeV, and neutrino number densities  $n_{\nu_e} = 3 \times 10^{33}$  cm<sup>-3</sup>,  $n_{\bar{\nu}_e} = 2.5 \times 10^{33}$  cm<sup>-3</sup>, and  $n_{\nu_x} = n_{\bar{\nu}_x} = 1 \times 10^{33}$  cm<sup>-3</sup>. Since the calculation is monochromatic, an energy  $E_\nu = 20$  MeV is used for all (anti)neutrinos regardless of flavor. The electron fraction implied by these values is  $Y_e \cong 0.13$ , and the oscillation potentials are  $\omega \cong 0.3$  km<sup>-1</sup>,  $\mu|\mathbf{D}(0)| \cong 3 \times 10^5$  km<sup>-1</sup>, and  $\lambda \cong 5 \times 10^7$  km<sup>-1</sup>. The last of these is implemented in the calculation using a matter-suppressed mixing angle  $\theta = 10^{-6}$  [17]. The mass hierarchy is not important for the results of this paper.

Crucially, this region is envisioned as being in the spatially extended atmosphere in which neutrinos decouple. NC scattering on neutrons is the dominant process affecting the heavy-lepton flavors. Using the fiducial values of the previous paragraph, the rate is estimated to be

$$\frac{1}{\lambda_{\nu n}} \sim \frac{n_n \sigma_0}{4} \left( \frac{1 + 3g_A^2}{4} \right) \left( \frac{E_\nu}{m_e} \right)^2 \sim \frac{1}{1.93 \text{ km}}, \quad (8)$$

where  $n_n$  is the neutron density,  $m_e$  is the electron rest mass,  $g_A \cong -1.28$  is the axial-vector coupling constant, and  $\sigma_0 = 4G_F^2 m_e^2 / \pi$  [19]. Corrections from inelasticity, recoil, and weak magnetism are ignored. NC scattering on protons is subdominant, and four-neutrino processes,  $\nu\bar{\nu}$  annihilation to  $e^+e^-$ , nucleon–nucleon bremsstrahlung, and the flavor-blind contribution from electron scattering are all calculated to be insignificant. While  $\nu n$  scattering is included in the calculation producing Fig. 1, as expected it has no effect (because, again, this model is isotropic and single-energy). The important point is that, in this representative calculation,  $\nu_x$  and  $\bar{\nu}_x$  continue to scatter but are no longer chemically coupled.

In contrast, CC capture on nucleons remains relevant:

$$\begin{aligned} \frac{1}{\lambda_{\nu_e n}^{\text{abs}}} &\sim n_n \sigma_0 \left( \frac{1 + 3g_A^2}{4} \right) \left( \frac{E_\nu + Q}{m_e} \right)^2 \left( 1 + 1.1 \frac{E_\nu}{m_n} \right) \\ &\sim \frac{1}{0.417 \text{ km}} \\ \frac{1}{\lambda_{\bar{\nu}_e p}^{\text{abs}}} &\sim n_p \sigma_0 \left( \frac{1 + 3g_A^2}{4} \right) \left( \frac{E_\nu - Q}{m_e} \right)^2 \left( 1 - 7.1 \frac{E_\nu}{m_n} \right) \\ &\sim \frac{1}{4.36 \text{ km}}, \end{aligned} \quad (9)$$

where  $Q = m_n - m_p$  and corrections from recoil and weak magnetism have been retained [19]. These rates are the critical ones in the collisionally unstable evolution. Electron scattering is secondary to CC capture, but it

makes the leading contributions to  $\Gamma_{e,x}^{CC}$  and  $\bar{\Gamma}_{e,x}^{CC}$ . Using the cross sections [20]

$$\sigma_{\nu_\alpha e} = \frac{3}{8} \sigma_0 c_{\nu_\alpha} \frac{(T + \frac{1}{4} \mu_e) E_\nu}{m_e^2} \quad (10)$$

with  $c_{\nu_e} \cong 2.21$ ,  $c_{\bar{\nu}_e} \cong 0.93$ , and  $c_{\nu_x} = c_{\bar{\nu}_x} \cong 0.36$ , the rates of (flavor-resolving) electron scattering are estimated to be

$$\begin{aligned} \frac{1}{\lambda_{\nu_e e}} &\sim n_{e^-} (\sigma_{\nu_e e} - \sigma_{\nu_x e}) \sim \frac{1}{11.4 \text{ km}} \\ \frac{1}{\lambda_{\bar{\nu}_e e}} &\sim n_{e^-} (\sigma_{\bar{\nu}_e e} - \sigma_{\bar{\nu}_x e}) \sim \frac{1}{37.2 \text{ km}}. \end{aligned} \quad (11)$$

On the basis of Eq. (5) and the interaction rates, we expect Fig. 1 to show flavor transformation on a timescale of  $\mathcal{O}(10)$   $\mu$ s. Indeed, collisional instability sets in just after  $\sim 20$   $\mu$ s, causing the  $\nu_e$ – $\nu_x$  coherence density to rise and the electron-flavor species to convert to the heavy-flavor ones (and vice versa). If  $\Gamma$  and  $\bar{\Gamma}$  are artificially set to a common value (*e.g.*, the average of their actual values), oscillations are stable and strongly matter-suppressed, and the amount of flavor conversion is utterly negligible. Thus all of the flavor evolution seen in Fig. 1 is due to the collisional instability associated with  $\Gamma \neq \bar{\Gamma}$ .

Following the initial conversion of flavor,  $n_{\nu_e}$  and  $n_{\bar{\nu}_e}$  return to their initial values due to ongoing emission from  $e^\pm$  capture on nucleons. As this takes place,  $n_{\nu_x}$  and  $n_{\bar{\nu}_x}$  are essentially frozen in place because of their inefficient chemical coupling. The species-dependence of the collision rates is therefore doubly important. It not only destabilizes the flavor field but also differentially restores (classical) equilibrium. In effect, the conversion of  $\nu_e$ ,  $\bar{\nu}_e$  into  $\nu_x$ ,  $\bar{\nu}_x$  hides these particles from absorption, allowing for an overall enhancement of the neutrino luminosity.

As for the prevalence, we are now equipped to make several comments. The obvious statement is that collisional instabilities are only noteworthy in regions where neutrinos are not yet fully free-streaming. At the other extreme, they are unlikely to occur in neutrino-trapping regions, where degeneracy decrees a stabilizing hierarchy  $n_{\nu_e} > n_{\nu_x} > n_{\bar{\nu}_e}$ . The favored region has neutrinos *partially* coupled to the medium, as in the fiducial case above.

To be more quantitative, where  $\Gamma$  and  $\bar{\Gamma}$  are well approximated by the rates of capture on nucleons, the critical electron fraction  $Y_e^{\text{crit}}$  (such that  $Y_e \lesssim Y_e^{\text{crit}}$  is unstable) can be found from the relation

$$Y_e^{\text{crit}} \cong \left( 1 + \frac{1}{\xi \mathcal{R}} \right)^{-1}. \quad (12)$$

This follows from Eq. (6) and  $\lambda_{\bar{\nu}_e p}^{\text{abs}} / \lambda_{\nu_e n}^{\text{abs}} \cong \xi n_n / n_p$ , where  $\xi$  depends on the neutrino energy spectra. Fig. 2 shows  $Y_e^{\text{crit}}$  with  $\xi = 1.6$ , consistent with the monochromatic approximation ( $E_\nu = 20$  MeV) used throughout this paper. A more comprehensive version of this analysis could

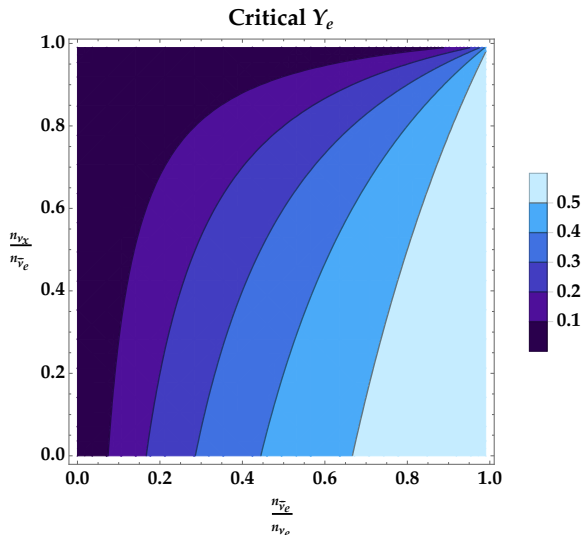


FIG. 2. The critical electron fraction  $Y_e^{\text{crit}}$  below which the system is predicted to be collisionally unstable, shown as a function of  $n_{\nu_x}/n_{\bar{\nu}_e}$  and  $n_{\bar{\nu}_e}/n_{\nu_e}$  and assuming  $n_{\nu_x} = n_{\bar{\nu}_x}$ . Since  $Y_e \lesssim 0.2$  is typical in the neutrino decoupling region, the majority of this parameter space is unstable.

be done by specifying spectral information, but the conclusion is anticipated to be the same: collisional instability is likely to occur in some regions.

*Extending the analysis.*—A curious feature of Eq. (5) is that it exhibits no dependence *at all* on oscillation parameters. A system with  $\omega = \mu = 0$  should therefore support the same solutions, assuming the initial state is seeded with flavor coherence. As a matter of fact, such a system does enter into the decay mode, but never into the growing one. From the vantage point of Eq. (5), the significance of the oscillation terms is that they cause the polarization vectors to wander through different configurations in flavor space until chancing upon the growing solution. Fast instabilities, by way of contrast, really can arise with  $\omega = 0$  as long as coherence is seeded. The  $\mu$  terms serve double duty in those cases, prompting the exploration of flavor space and driving the instabilities themselves.

Linear stability analysis provides a complementary perspective. For this we return to the density matrices. Linearizing in off-diagonal elements and adopting a matter-suppressed mixing angle  $\theta_m \cong 0$ ,

$$\begin{aligned} i\partial_t \rho_{ex} &= \left( -\omega - \sqrt{2}G_F(n_{\bar{\nu}_e} - n_{\bar{\nu}_x}) - i\bar{\Gamma} \right) \rho_{ex} \\ &\quad + \sqrt{2}G_F(n_{\nu_e} - n_{\nu_x}) \bar{\rho}_{ex} \\ i\partial_t \bar{\rho}_{ex} &= \left( +\omega + \sqrt{2}G_F(n_{\nu_e} - n_{\nu_x}) - i\bar{\Gamma} \right) \bar{\rho}_{ex} \\ &\quad - \sqrt{2}G_F(n_{\bar{\nu}_e} - n_{\bar{\nu}_x}) \rho_{ex}. \end{aligned} \quad (13)$$

Seeking collective modes, we now take  $\rho_{ex} = Qe^{-i\Omega t}$  and  $\bar{\rho}_{ex} = \bar{Q}e^{-i\Omega t}$ . The dispersion relation results from plugging these expressions into Eqs. (13) and dispensing with

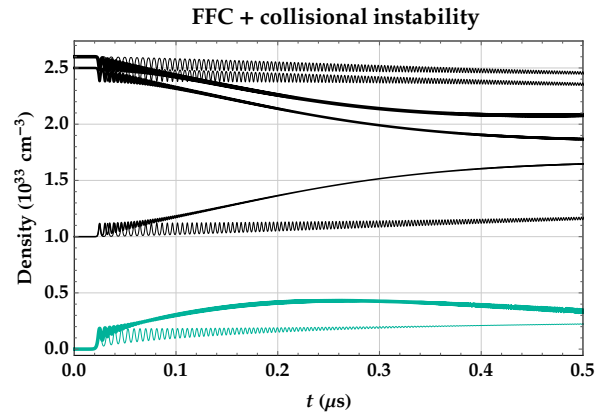


FIG. 3. Collisionally and fast-unstable evolution in an anisotropic calculation:  $n_{\nu_e}$  (thick black curve),  $n_{\bar{\nu}_e}$  (medium),  $n_{\nu_x}$  (thin), and neutrino coherence density  $|\mathbf{P}_T|/2$  (teal). The very thin curves, which show only minor secular change, are the results when  $\Gamma$  and  $\bar{\Gamma}$  are artificially set to the average of their actual values (hence  $\Gamma = \bar{\Gamma}$ ). The rapid oscillatory motion is the swinging of the fast pendulum [21]. No conversion would be visible if the system were stable to fast flavor conversion (FFC).

$Q$  and  $\bar{Q}$ . It can be solved analytically:

$$\text{Im } \Omega \cong \pm \frac{\Gamma - \bar{\Gamma}}{2} \frac{\mu S}{\sqrt{(\mu D)^2 + 4\omega\mu S}} - \frac{\Gamma + \bar{\Gamma}}{2}, \quad (14)$$

where  $S = |\mathbf{S}(0)| = n_{\nu_e} - n_{\nu_x} + n_{\bar{\nu}_e} - n_{\bar{\nu}_x}$  and  $D = |\mathbf{D}(0)| = n_{\nu_e} - n_{\nu_x} - n_{\bar{\nu}_e} + n_{\bar{\nu}_x}$ . ( $\mathbf{S}$  and  $\mathbf{D}$  are assumed to point along  $\mathbf{z}$  initially, but the formulas are easily adapted.) If  $\mu D \gg 2\sqrt{\omega\mu S}$ , which is usually expected of the setting we have in mind, then the instability criterion coincides with Eq. (6). If  $\mu D < 2\sqrt{\omega\mu S}$  and  $\omega < 0$  (indicating the inverted hierarchy), then Eq. (14) is invalidated by intervention of the bipolar instability.

Up to this point the analysis has assumed monochromaticity, isotropy, and homogeneity. The first of these is justified by the high neutrino density. Though not presented here, numerical calculations with multiple energies confirm that collisional instability affects them collectively.

Calculations also confirm the presence of collisionally unstable evolution in anisotropic set-ups. An interesting case is one where collisional and fast instabilities are present together. Fig. 3 shows the results of such a calculation. The parameters are the same as those used in making Fig. 1 except that  $n_{\nu_e}$  has been decreased to  $2.6 \times 10^{33} \text{ cm}^{-3}$  and the angular distributions have been made anisotropic, so as to make the system unstable to fast oscillations. As with the other parameters, the angular distributions are chosen to be representative of real conditions in a supernova. They are specified by the flux factors (*i.e.*, the ratios of energy flux to energy density)  $f_{\nu_e} = 0.05$ ,  $f_{\bar{\nu}_e} = 0.10$ , and  $f_{\nu_x} = f_{\bar{\nu}_x} = 0.15$ . Radiative pressures are prescribed using M1 closure [22]. These dis-

tributions are nearly isotropic and are plotted in Fig. 1 of Ref. [23].

The onset of fast flavor conversion prompts the growth of the collisional instability on a much shorter timescale than was seen in Fig. 1. Furthermore, significantly greater flavor transformation occurs when  $\Gamma \neq \bar{\Gamma}$  than when  $\Gamma = \bar{\Gamma}$ , testifying to the fact that the results observed in Fig. 3 are not simply caused by decoherence. In a more realistic setting, collisional relaxation will compete with various forms of collisionless relaxation [24, 25] to determine the outcome. Nonetheless, the figure demonstrates that collisional instability has the potential to be enhanced by fast oscillations rather than wiped out by them.

Lastly, collisional instability is expected to occur in homogeneous and inhomogeneous environments alike, much as the bipolar instability is known to. In fact, preliminary evidence points to the collisional instability identified here—a homogeneous, isotropic, temporally growing mode—as one member of a family. These remarks need further development, however, and will be presented in a future publication.

*Added note.*—Since the first version of this paper appeared, subsequent work has expanded on its major points [26–30].

*Acknowledgements.*—Support for this work was provided by NASA through the NASA Hubble Fellowship grant number HST-HF2-51461.001-A awarded by the Space Telescope Science Institute, which is operated by the Association of Universities for Research in Astronomy, Incorporated, under NASA contract NAS5-26555.

---

\* NASA Einstein Fellow (ljohns@berkeley.edu)

- [1] A. Mirizzi, I. Tamborra, H.-T. Janka, N. Saviano, K. Scholberg, R. Bollig, L. Hudepohl, and S. Chakraborty, Supernova Neutrinos: Production, Oscillations and Detection, *Riv. Nuovo Cim.* **39**, 1 (2016).
- [2] A. Banerjee, A. Dighe, and G. Raffelt, Linearized flavor-stability analysis of dense neutrino streams, *Phys. Rev. D* **84**, 053013 (2011).
- [3] I. Izaguirre, G. Raffelt, and I. Tamborra, Fast pairwise conversion of supernova neutrinos: A dispersion relation approach, *Phys. Rev. Lett.* **118**, 021101 (2017).
- [4] F. Capozzi, B. Dasgupta, E. Lisi, A. Marrone, and A. Mirizzi, Fast flavor conversions of supernova neutrinos: Classifying instabilities via dispersion relations, *Phys. Rev. D* **96**, 043016 (2017).
- [5] R. F. Sawyer, Neutrino cloud instabilities just above the neutrino sphere of a supernova, *Phys. Rev. Lett.* **116**, 081101 (2016).
- [6] S. Chakraborty, R. Hansen, I. Izaguirre, and G. Raffelt, Collective neutrino flavor conversion: Recent developments, *Nucl. Phys.* **B908**, 366 (2016).
- [7] I. Tamborra and S. Shalgar, New developments in flavor evolution of a dense neutrino gas, arXiv:2011.01948 (2020).
- [8] H. Duan, G. M. Fuller, and Y.-Z. Qian, Collective neutrino oscillations, *Ann. Rev. Nucl. Part. Sci.* **60**, 569 (2010).
- [9] B. H. J. McKellar and M. J. Thomson, Oscillating neutrinos in the early universe, *Phys. Rev. D* **49**, 2710 (1994).
- [10] A. D. Dolgov, Neutrino oscillations in the early universe. resonant case, *Nucl. Phys.* **B610**, 411 (2001).
- [11] S. Hannestad, R. S. Hansen, T. Tram, and Y. Y. Wong, Active-sterile neutrino oscillations in the early universe with full collision terms, *J. Cosmol. Astropart. Phys.* **2015** (08), 019.
- [12] L. Johns, Derivation of the sterile neutrino boltzmann equation from quantum kinetics, *Phys. Rev. D* **100**, 083536 (2019).
- [13] S. A. Richers, G. C. McLaughlin, J. P. Kneller, and A. Vlasenko, Neutrino quantum kinetics in compact objects, *Phys. Rev. D* **99**, 123014 (2019).
- [14] F. Capozzi, B. Dasgupta, A. Mirizzi, M. Sen, and G. Sigl, Collisional triggering of fast flavor conversions of supernova neutrinos, *Phys. Rev. Lett.* **122**, 091101 (2019).
- [15] S. Shalgar and I. Tamborra, Change of direction in pairwise neutrino conversion physics: The effect of collisions, *Phys. Rev. D* **103**, 063002 (2021).
- [16] J. D. Martin, J. Carlson, V. Cirigliano, and H. Duan, Fast flavor oscillations in dense neutrino media with collisions, *Phys. Rev. D* **103**, 063001 (2021).
- [17] S. Hannestad, G. G. Raffelt, G. Sigl, and Y. Y. Y. Wong, Self-induced conversion in dense neutrino gases: Pendulum in flavor space, *Phys. Rev. D* **74**, 105010 (2006).
- [18] L. Johns and G. M. Fuller, Strange mechanics of the neutrino flavor pendulum, *Phys. Rev. D* **97**, 023020 (2018).
- [19] A. Burrows, S. Reddy, and T. A. Thompson, Neutrino opacities in nuclear matter, *Nucl. Phys. A* **777**, 356 (2006), special Issue on Nuclear Astrophysics.
- [20] R. L. Bowers and J. R. Wilson, A numerical model for stellar core collapse calculations, *Astrophys. J. Suppl. Ser.* **50**, 115 (1982).
- [21] L. Johns, H. Nagakura, G. M. Fuller, and A. Burrows, Neutrino oscillations in supernovae: Angular moments and fast instabilities, *Phys. Rev. D* **101**, 043009 (2020).
- [22] L. Johns and H. Nagakura, Fast flavor instabilities and the search for neutrino angular crossings, (2021), arXiv:2104.04106 [hep-ph].
- [23] L. Johns and H. Nagakura, Self-consistency in models of neutrino scattering and fast flavor conversion (2022), arXiv:2206.09225 [hep-ph].
- [24] L. Johns, H. Nagakura, G. M. Fuller, and A. Burrows, Fast oscillations, collisionless relaxation, and spurious evolution of supernova neutrino flavor, *Phys. Rev. D* **102**, 103017 (2020).
- [25] S. Bhattacharyya and B. Dasgupta, Fast flavor depolarization of supernova neutrinos, *Phys. Rev. Lett.* **126**, 061302 (2021).
- [26] L. Johns and Z. Xiong, Collisional instabilities of neutrinos and their interplay with fast flavor conversion in compact objects, *Phys. Rev. D* **106**, 103029 (2022).
- [27] I. Padilla-Gay, I. Tamborra, and G. G. Raffelt, Neutrino fast flavor pendulum. ii. collisional damping, *Phys. Rev. D* **106**, 103031 (2022).
- [28] Y.-C. Lin and H. Duan, Collision-induced flavor instability in dense neutrino gases with energy-dependent scattering, arXiv preprint arXiv:2210.09218 (2022).
- [29] Z. Xiong, M.-R. Wu, G. Martínez-Pinedo, T. Fischer, M. George, C.-Y. Lin, and L. Johns, Evolution of colli-

sional neutrino flavor instabilities in spherically symmetric supernova models, arXiv preprint arXiv:2210.08254 (2022).

[30] Z. Xiong, L. Johns, M.-R. Wu, and H. Duan, Collisional

flavor instability in dense neutrino gases, arXiv preprint arXiv:2212.03750 (2022).